Check for updates

Ultra-efficient highly-selective MFC-7 cancer cell therapy enabled by combined electric-pulse carbon 1D-nanomaterials platforms†

Sophia S. Y. Chan, [ID] [a] Shao Xiang Go,[a] Maria Prisca Meivita, [ID] [a] Denise Lee, [ID] [a] Natasa Bajalovic [ID] *[a] and Desmond K. Loke [ID] *[ab]

Advancements in technology are enabling early cancer treatments, improving patient survivability in some types of cancers. Electrothermal cancer therapy offers numerous advantages such as high efficiency and minimal invasiveness. However, traditional electrothermal nanoagents has been limited by unresolved concerns including poor cell-selectivity and weak contrast in ablation efficiency between healthy and cancer cells. Here, we control thermal distributions of cell systems using combined electrical-pulse carbon one-dimensional (1D-) nanomaterial platforms *via* Joule heating effects. We then proposed the electrothermal ablation of cancer cells using integrated alternating-current (AC-) pulse carbon-nanotube (CNT) platforms. Electrothermal simulations reveal an increased peak temperature for an extended stimulation time within the cell layers in the presence of CNT. Moreover, experiments show a significant difference in CNT biocompatibility between healthy breast epithelial (MCF-10A) cells and luminal breast cancer (MCF-7) cells. Additionally, electrothermal ablation was observed to be enhanced in MCF-7 cells, while cell viability was maintained in MCF-10A cells under the same conditions. Furthermore, a ~68% decrease in cell viability was achieved after applying AC pulses, above an average of ~40% decrease in cell viability for existing carbon-based photothermal nanoagents without additional chemotherapeutic drugs. This previously unreported combination of CNT nanomaterials and electrical stimulation represents an approach to unlocking the ultra-efficient electrothermal ablation of MCF-7 cells and provides a promising avenue for cancer treatment.

Introduction

Advancements in technology are enabling earlier treatments for achieving enhanced patient survivability in some types of cancer. However, with more than 10 million cancer related deaths worldwide in 2020 alone,[1] much work needs to be done to improve survival rates. Moreover, the Covid-19 pandemic has forced cancer units to modify their operations to mitigate the risk of viral spread while continuing cancer therapy. As a result, research has been focused on developing alternative and adjunct therapies for early cancer treatments to reduce the number of cancer-related deaths. Traditional cancer treatments such as chemotherapy and radiotherapy can be limited by poor selectivity, resulting in low dosages reaching the tumor site

with adverse side effects.[2–4] Recently, research efforts are pursuing next-generation therapies such as thermal ablative therapies, which can be used in combination with current cancer treatments to reduce cancer recurrence and improve patient outcome.[3,5,6] These methods typically rely on an energy source to produce heat in excess of 42 °C (hyperthermia) to ablate cancer cells,[7–9] and are advantageous for being mini-mally invasive. Traditional sources of applying heat to ablate cells/tissues rely on radiofrequency (RF) current, ultrasound or lasers.[6,10] For example, RF ablation is a promising alternative to surgery due to advancements in medical technology.[11] The energy dispersed by the electrodes is capable of heating the cells locally, resulting in a controlled cell death;[12] RF ablation for thyroid tumors demonstrated good patient outcomes and with little/no recurrence.[13] In addition, photothermal therapies (PTT) based on light are a promising therapeutic strategy for ablating cancer cells without affecting neighbouring healthy cells; they provide a localised and non-invasive approach, with the capability of cell-specific targeting to minimise side-effects.[2,4,10,14] Nanomaterials harnessed in PTT are able to convert optical light in the near infrared (NIR) range into heat

[a] Department of Science, Mathematics and Technology, Singapore University of Technology and Design, Singapore 487372, Singapore.
E-mail: natasa_bajalovic@sutd.edu.sg, desmond_loke@sutd.edu.sg
[b] Office of Innovation, Changi General Hospital, Singapore 529889, Singapore
† Electronic supplementary information (ESI) available. See DOI: 10.1039/d1ma01118a

to ablate cancer cells.[4,8,15] Moreover, their high surface-area-to-volume ratio allow for easy functionalisation that can fine tune their properties such as solubility and dispersion to improve cytotoxicity, and provide cell-specific targeting, making them clinically relevant.[14,16–19] Thus, nanomaterials with unique characteristics have been of interest for developing new therapeutic applications.

Carbon nanotubes (CNT) are one dimensional (1D) nanomaterials that have shown great promise for biological applications. The nanotubes are comprised of hexagonal, sp^2 hybridised carbon (C) sheets rolled into nanotubes and possess characteristics similar to graphene.[20] In particular, CNTs have a unique band gap structure that result in excellent mechanical, thermal, electrical and optical properties, which can be tuned by CNT structure (*e.g.* single or multi-walled CNT, chirality, nanotube length and diameter, *etc.*)[20–23] Moreover, CNTs have unique photocurrent properties that allow for enhanced current flow when exposed to light; CNTs have a strong optical absorption within the NIR range. They have been utilised in a wide range of optoelectronic applications such as photoconductors, photoresistors, photodetectors and other applications.[22,23]

Besides, CNTs have been harnessed for PTT in combination with other cancer therapeutic approaches;[2,24–26] CNTs are biologically compatible and are able to convert non-toxic NIR wavelengths into heat for ablating cancer cells. In addition, CNTs have demonstrated high thermal and electrical conductivities due to their unique 1D structure.[27,28] Altering the CNT structure can influence both electrical and thermal conductivities; studies suggest that higher CNT aspect ratios result in increased thermal conductivities.[29–31] Furthermore, scaffolds comprised of CNT networks also demonstrate different mechanical, electrical and thermal properties.[32,33] As a result, CNT has been used for Joule heating applications.[33,34] However, such applications of CNT for cancer cell-specific electrothermal ablation have yet to be explored. Thus, it is our interest to control the thermal distributions of cells for the ablation of cancer cell using a CNT AC-pulse platform.

Here, we alter the thermal distributions of cell systems using combined electrical-pulse 1D-nanomaterial platforms *via* Joule heating effects. We propose an electrothermal method to thermally ablate breast cancer cells using an integrated alternating-current (AC) pulse CNT platform. Electrothermal simulations elucidate an increase in peak temperature for an extended stimulation period within the cell layers in the presence of CNT. Further experiments illustrate a difference in CNT biocompatibility between healthy breast epithelial (MCF-10A) cells and luminal breast cancer (MCF-7) cells. Moreover, electrothermal ablation was observed to be enhanced in MCF-7 cells, while cell viability was maintained in MCF-10A cells under the same conditions, potentially enhancing treatment safety. Furthermore, a $\sim$68% decrease in cell viability was achieved upon AC pulse application in the presence of CNT, which is above an average of $\sim$40% decrease in cell viability for current carbon-based photothermal nanoagents without additional chemotherapeutic drugs. This previously unreported methodology based on CNT materials for electrothermal cancer cell ablation holds great potential for the development of efficient therapeutic options, which can be further applied for clinical purposes.

Experimental section

Electrothermal simulations

Electrothermal simulations were performed in ANSYS software *via* finite element method (FEM). We constructed a model of the electrothermal-therapy platforms with cells (Fig. S1a, ESI†). The model comprised two 650 nm thick left and right indium tin oxide (ITO) electrodes on a glass substrate. Different distances between the electrodes (50, 100, 150 and 200 μm) were investigated, and an active region was formed between the electrodes. The active region consisted of either a pure cell layer (control model) or a cell-CNT-cell layer (model with CNT) (Fig. S1a, ESI†). The dimensions of the model and parameters of the materials used are shown in Tables S1 and S2 (ESI†), respectively. For the simulations, material parameters were assumed to be independent of temperature, with the initial temperature set at 310 K. Heat transfer was modelled using the heat-conduction equation

$$k\nabla^2 T + q = \rho c \frac{\partial T}{\partial t} \tag{1}$$

where k is thermal conductivity, t is time, T is temperature, q is the internal heat inside a volume, ρ is the density of the material and c is the specific heat of the material. A single, square bias-voltage pulse (pulse width = 1 ms) was applied with different amplitudes (1, 5 and 10 V), and peak temperature within the cell layers were computed.

CNT preparation and characterization

To prepare the nanomaterials for characterisation, CNT in deionised (DI) water (1 wt%, US4120W, US Research Nanomaterials) was sonicated (Elmasonic, S130H) for $\sim$20 min at room temperature (RT). CNT was then drop casted onto silicon (Si) substrate in preparation for material characterisation. Transmission electron microscopy (TEM) was performed using a transmission electron microscope (FEI Talos F200, Thermo Scientific). The accelerating voltage was fixed at 200 kV. Raman testing was performed using a Raman microscope (Renishaw inVia) with a 532 nm excitation laser. The measured wave number range was 100–3000 cm^{-1}. The X-ray photoelectron spectroscopy (XPS) data were collected using an XPS spectrometer (PHI-5400, Physical Electronics, US) with an Al Ka beam source (250 W) and positron-sensitive detector (PSD). The binding energy resolution is 0.8 eV, angle resolution is 45° and detection limit is 80 K counts per second (CPS). The base pressure of the measurement chamber was set to 3.0×10^{-7} Pa, and the Ar ion (voltage of 12 kV, current of 4.2 mA) sputtering speed is 0.28 nm s^{-1} over an area of 400×400 μm^2. Prior to incubation with cells, CNTs were sonicated as described above.

Cell culture

Healthy breast epithelial (MCF-10A) cells were cultured in Dulbecco's Modified Eagle Media supplemented with Ham's F12 (DMEM/F12, 11320033), fetal bovine serum (FBS, 10%, 26140079), epidermal growth factor (EGF, 20 ng mL^{-1}, PHG0311L, Gibco), hydrocortisone (0.5 μg mL^{-1}, H0888-1G) and insulin (10 μg mL^{-1}, 12585014, Sigma). Luminal breast cancer (MCF-7) cells were cultured in DMEM (08458-45, Nacalai Tesque) enriched with FBS (7%, Gibco). Both cell lines were maintained at 37 °C in a 5% CO$_2$ atmosphere.

System setup

Two indium tin oxide (ITO) left and right electrodes were deposited on a glass substrate (Latech). The cloning cylinder (C3983-50EA, Sigma) was then adhered to the ITO substrate with a silicone adhesive (Fig. 1a). The system was sterilised under ultraviolet (UV) light for 5 min before the wells were filled with pure ethanol (EtOH, E7023-1L, Sigma) for 20 min. After removing EtOH, the wells were rinsed with Dulbecco's phosphate buffer solution (DPBS, 14190235, Gibco) prior to cell seeding. The proposed system can be reused. After electrothermal ablation, the ITO substrate and cloning cylinder were soaked in bleach for more than 24 h. The components were then rinsed with water, and the residual silicone adhesive was removed mechanically. They were then sonicated in a mixture of soap and water before rinsing them with EtOH, and left to dry in an oven (60 °C) before use.

Electrical ablation

MCF-10A cells and MCF-7 cells ($\sim 3 \times 10^3$ cells) were seeded in the set up for at least $\sim$24 h before material addition to achieve $\sim$70% confluency. After incubating with CNT for $\sim$24 h, cells were electrically stimulated using the semiconductor characterisation system (Keithly 4200-SCS). Square alternating current (AC) pulses were applied to electrothermally ablate the cells (amplitude = 10 V, pulse width = 1 ms, number of pulses = 10). A figure of the electrical wave profile is provided in Fig. S2 (ESI†). Cells were exposed to a microscope light during electrical stimulation ($\sim$500 nm, $\sim$640 lm, eVue III 10×).

Cell viability testing

For detection of CNT cytotoxicity, MCF-10A cells and MCF-7 cells ($\sim 3 \times 10^3$ cells) were seeded in 96 well plates. After $\sim$24 h of incubation, different concentrations of CNT (0, 5, 10, 20 and 30 μg mL^{-1}) were added to the wells. Cell viability was determined for t = 24 h and 48 h using a WST-1 assay (10%, 11644807001, Sigma). Absorbance was read at λ = 450 nm (Multiskan GO, 1510-03742C) after $\sim$4 h of cell incubation. The WST-1 assay was also utilised to determine cell viability after applying the electrical pulse. Propidium iodide (PI, P1304MP, Gibco) was used to confirm the extent of cell death after material addition and electrical pulse. After electrical stimulation ($\sim$24 h), cells were incubated with PI (1 μM) for $\sim$1 h and fixed with 3.7% of paraformaldehyde
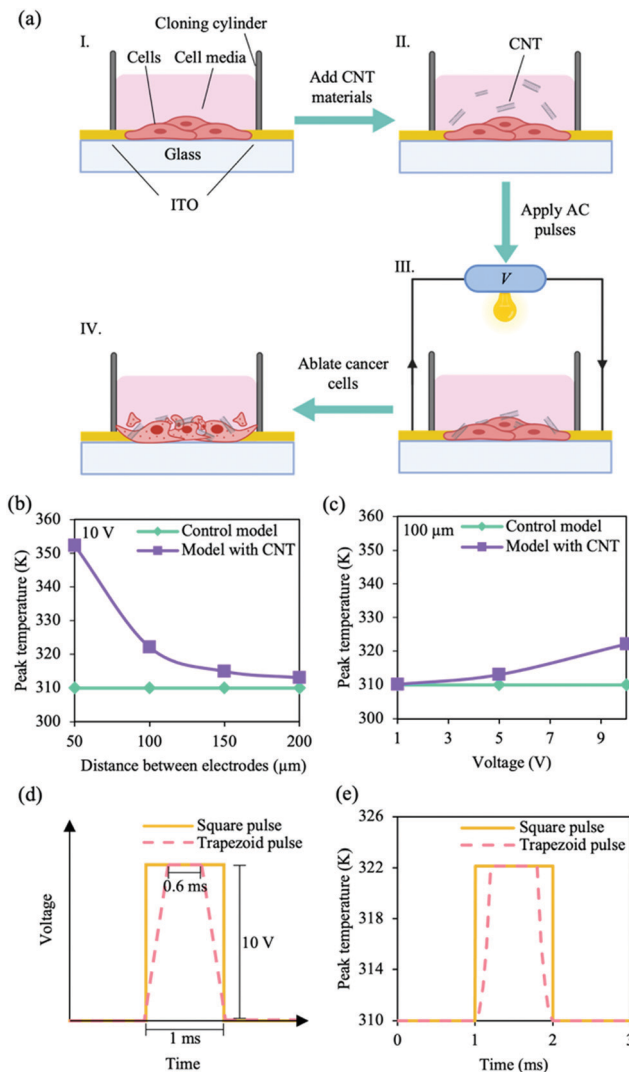

Fig. 1 A combined electrothermal therapy platform based on AC pulses and CNT materials and electrothermal simulations. (a) A step-by-step illustration of the proposed method. I. After adhering the cloning cylinder to the ITO glass substrate with a silicone adhesive, MCF-10A cells or MCF-7 cells ($\sim 3 \times 10^3$ cells) were seeded within the set up. II. CNT was added to the cells $\sim$24 h after seeding. III. AC pulses (amplitude = 10 V, pulse width = 1 ms, number of pulses = 10) were applied to the cells. IV. Cell death was observed. (b) Variations of simulated peak temperatures for the cell layer without CNT (control model, green) and with CNT (model with CNT, purple) for different distances between the electrodes (50, 100, 150 and 200 μm) at an applied voltage of 10 V. (c) Simulated peak temperature of the control model and model with CNT (green and purple, respectively) for different bias voltages. The distance between the electrodes was set at 100 μm. The temperature profiles of the model with CNT is dependent on the shape of electrical pulses; (d) Schematic illustration of bias waveforms of the square bias-voltage pulse (pulse width = 1 ms, yellow) and trapezoid bias-voltage pulse (pulse width = 0.6 ms, pink) with an amplitude of 10 V. (e) The results show temperature profiles for the model with CNT under applied square pulse (yellow) and trapezoid pulse (pink), with the electrode distance chosen to be 100 μm.

(PFA, F8775-15ML, Sigma) before imaging (10×, Olympus DP22). Images were processed using Fiji software.[35]

Results

Methodology of a combined AC pulse CNT platform

We adopted a strategy to efficiently electrothermally ablate luminal breast cancer (MCF-7) cells using an alternating current (AC) pulse CNT platform shown in Fig. 1a. A glass substrate was used as the starting material, on which two 650 nm thick indium tin oxide (ITO) left and right electrodes were deposited for external circuitry connections. The distance between the electrodes was chosen to be ~ 100 μm. A cloning cylinder was then secured with a silicone adhesive on the substrate, and the circuit was closed by seeding MCF-10A cells or MCF-7 cells ($\sim 3 \times 10^3$ cells) within the system. Finally, CNTs were added to the system to enhance thermal distribution. AC pulses were applied to electrothermally ablate the cancer cells. The efficiency of electrothermal ablation was then determined by investigating cell viability.

Due to their unique one dimensional (1D) structure, CNTs have demonstrated a high thermal conductivity.[27,28] Thermal conductivity can be governed by electronic carriers (electrons and holes), lattice vibrations (phonons) and other excitations.[36,37] Depending on their chirality (n, m), CNTs can exhibit metallic or semiconducting behaviours; CNT with arm-chair chirality ($n = m$) tend to be metallic, while zig-zag ($n = 0$, or $m = 0$) and chiral CNTs are semiconducting.[22,28,38] While phonon transport is the primary contributor of thermal conductivity in non-metallic materials, the small band gap (zero to ~ 1.5 eV) suggests that electronic carriers can also contribute to the thermal conductivity of the metal-like CNTs.[27,37] We hypothesise that applying an appropriate electrical pulse can cause Joule heating of the CNT, resulting in heating of the cancer cells and causing cell death.

We investigated the thermal distribution of the AC pulse CNT system using electrothermal simulations; we examined the effects of distance between electrodes and pulse amplitude on peak cell-layer temperature within the model. The initial temperature of the simulations were set at 310 K (~ 37 °C). When an electrical pulse was applied to the system (pulse length, 1 ms; different bias-voltages, 1, 5 and 10 V), temperature changes started within the CNT layer and propagated toward the surrounding cell layers (Fig. S1b, ESI†). No change in temperature was observed for the control model (Fig. 1b). Additionally, the peak temperature of the cell layer within the model with CNT was dependent on the distance between the electrodes and pulse amplitude (Fig. 1b and c). Upon the application of a 10 V pulse, while no significant changes were observed for the control model with different distances between the electrodes, a maximum peak temperature of ~ 352 K was observed for the model with CNT when the distance between electrodes was set at 50 μm (Fig. 1b). For an electrode width of 100 μm, we observed a maximum peak temperature of ~ 322 K for the model with CNT at 10 V (Fig. 1c), corresponding to a temperature change of ~ 12 K. Moreover, we observed that the shape of the electrical pulse can affect the rate of temperature change over time within the cell layers (Fig. 1d). The maximum temperature for the cell layers

was plotted as a function of time (Fig. 1e); a sharp increase/decrease in temperature was observed under an applied square bias-voltage pulse with a peak of ~ 322 K (the stimulation time at peak temperature is long). On the other hand, the temperature rise/fall was less steep under an applied trapezoid bias-voltage pulse (short stimulation time at peak temperature). Thus, a square-based stimulation and temperature increase of ~ 12 K could lead to peak temperatures of ~ 49 °C for an extended stimulation time within the cells. Since proteins and other cellular components start to denature at temperatures above 40 °C and exposure of cells to temperatures above 42 °C is sufficient for cell death,[7–9] we speculate that the maintaining a high temperature for a prolonged stimulation time using the AC pulse CNT system can result in a stronger cell ablation and lead to more cell death.

Characterisation and effects of CNT materials with cells

CNTs were synthesised *via* chemical vapour deposition (CVD). Before characterisation, CNT in DI water was sonicated (~ 20 min) and drop casted on silicon. The chemical composition of CNTs were investigated by X-ray photoelectron spectroscopy (XPS). The XPS spectra for the carbon (C) 1s orbital and the oxygen (O) 1s orbital are presented in Fig. 2a and b, respectively. For the C 1s orbital, a peak was observed at ~ 285 eV, typical for CNT. Another peak was observed at ~ 531 eV, characteristic for the O 1s orbital, which indicates that the CNT could have undergone oxidation in DI water. To investigate the crystal structure and quality of the CNT, Raman spectroscopy was performed (Fig. 2c). The Raman spectra reveals two distinct peaks at ~ 1588 cm^{-1} and ~ 1344 cm^{-1}, corresponding to the G and D bands, respectively. The G band is associated with the stretching vibrations along the nanotube axis (E_{2g} stretching), while the D band represents the oxygen defects in the CNT, which could be due to oxidation. Moreover, transmission electron microscopy (TEM) was carried out to investigate the morphology and dispersion of the CNTs (Fig. 2d). Tube-like features were observed, with defined carbon atoms forming the walls of individual tubes. Furthermore, the CNTs were disclosed to be hollow, coaxial, entangled, multi-walled and were observed to have an outer diameter of ~ 10 nm and inner diameter of ~ 5 nm (Fig. S3, ESI†), which is similar to that demonstrated in other studies.[39–41]

We investigated the cytotoxicity of CNT for both cell lines. After seeding MCF-10A cells and MCF-7 cells for ~ 24 h, different concentrations of CNT were added (0, 5, 10, 20 and 30 μg mL^{-1}) and cell viability was analysed at 24 and 48 h (Fig. 2e and f, respectively). For both cell lines, cell viability decreased with increasing CNT concentration and time. Moreover, CNT was observed to be more toxic for MCF-7 cells compared to MCF-10A cells; this was most evident after 48 h. To study the extent of cell viability as a result of concentration dependant electrothermal ablation, we selected CNT concentrations of 10 and 30 μg mL^{-1}. The selectivity of electrothermal ablation for MCF-7 cells over MCF-10A cells were also investigated at the selected CNT concentrations. CNT cytotoxicity is dependent on nanotube structure, length, diameter, surface
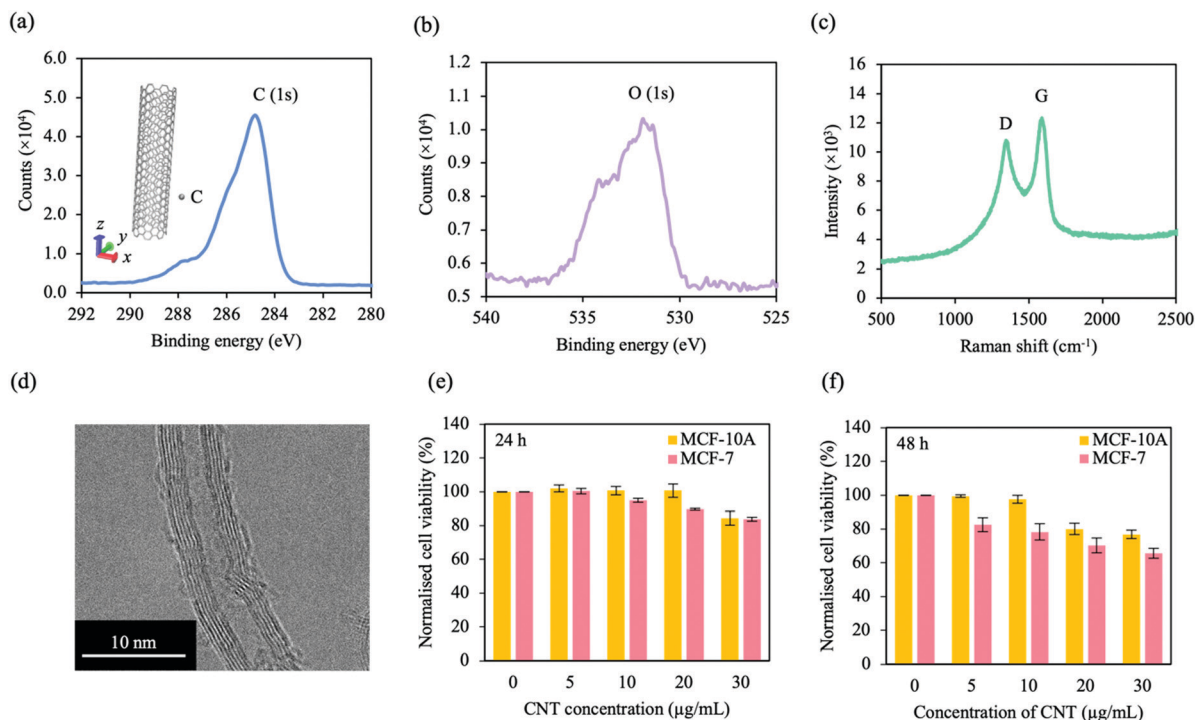
Fig. 2 Characterisation of CNT materials and cell interaction. XPS spectra of (a) the C 1s orbital and (b) O 1s orbital in CNT. An atomic structure of CNT (grey) is presented in the inset of (a). (c) Raman spectra of CNT with two peaks. The two peaks correspond to the D and G bands as labelled. (d) TEM image of CNT. Tube-like structures were observed with defined carbon atoms forming the walls. (e and f) CNT cytotoxicity for MCF-10A cells (yellow) and MCF-7 cells (pink) at (e) 24 h and (f) 48 h. Significance is presented in Table S3 (ESI†). Data is representative of mean ± SEM ($n = 6$ for 3 independent experiments).

chemistry and cell type.[42,43] While some of the previous works describe CNT to be cytotoxic, the results here show that cell viability is maintained at CNT concentrations within a range of 0 to 30 μg mL^{-1}. Other works show that low concentrations of CNT do not severely affect cell viability; Vittorio *et al.* show negligible toxic effects of human neuroblastoma cells (SH-SY5Y) at low CNT concentrations ($<$50 μg mL^{-1}),[44] while Shvedova *et al.* show similar cell viability results for human epidermal keratinocytes (HaCaT) at CNT concentrations of $\sim$120 μg mL^{-1}.[45] Similar to this work, time-dependant CNT cytotoxicity has also been observed; stem cell viability decreased with CNT concentration and time.[46]

Combined effects of AC pulses and CNT materials on ablating cancer cells

The combination of CNT and AC pulses to ablate cancer cells was investigated. Both MCF-10A cells and MCF-7 cells ($\sim$3 × 10^3 cells per well) were seeded $\sim$24 h before changing media or adding CNT (10 and 30 μg mL^{-1}) (MCF-10A/CNT and MCF-7/CNT, respectively). The electrical characterisation system has an upper bound of pulse amplitude of 10 V. From the simulation studies, a square electrical pulse with an amplitude of 10 V and pulse width of 1 ms was able to generate temperature changes of $\sim$12 K within the cell layer for an extended stimulation time (Fig. 1b and c), corresponding to temperatures in excess of 42 °C. Thus, based on the testing upper bounds and simulation results, we chose to apply 10 square AC pulses of

10 V with a pulse width of 1 ms under light conditions. After $\sim$24 h of material incubation, the cells were then electrically stimulated with AC pulses (10 pulses of 10 V with 1 ms pulse width, Fig. S2, ESI†).

Cell viability was measured $\sim$24 h after electrical application using a WST-1 assay; cells were incubated with 10% of WST-1 in media for 4 h prior to plate reading at $\lambda = 450$ nm. The measured intensity was normalised to control (no CNT incubation), and presented in Fig. 3a and b for MCF-10A cells and MCF-7 cells, respectively. Cell viability was maintained for MCF-10A/CNT with or without AC pulse stimulation compared with control (Fig. 3a); no significant changes were observed in cell viability regardless of CNT concentration. We observed that cell viability for MCF-7/CNT with AC pulses decreased substantially with increasing CNT concentration when normalised to control, observing maximum MCF-7 cell ablation when AC pulses were applied in the presence of 30 μg mL^{-1} CNT (10 μg mL^{-1}, $\sim$74%; 30 μg mL^{-1}, $\sim$32%; Fig. 3b). Cell viabilities were not affected by AC pulse exposure without CNT incubation (Fig. S4, ESI†). The percentage decrease in cell viability ($\Delta x_{\text{cell viability,\%}}$) was calculated using the following equation

$$\Delta x_{\text{cell viability,\%}} = \frac{n_{\text{cells}} - n_{\text{cells/CNT}}}{n_{\text{cells}}} \times 100\% \qquad (2)$$

where n_{cells} is the normalised cell viability for control with AC pulse, and $n_{\text{cells/CNT}}$ is the normalised cell viability for cells
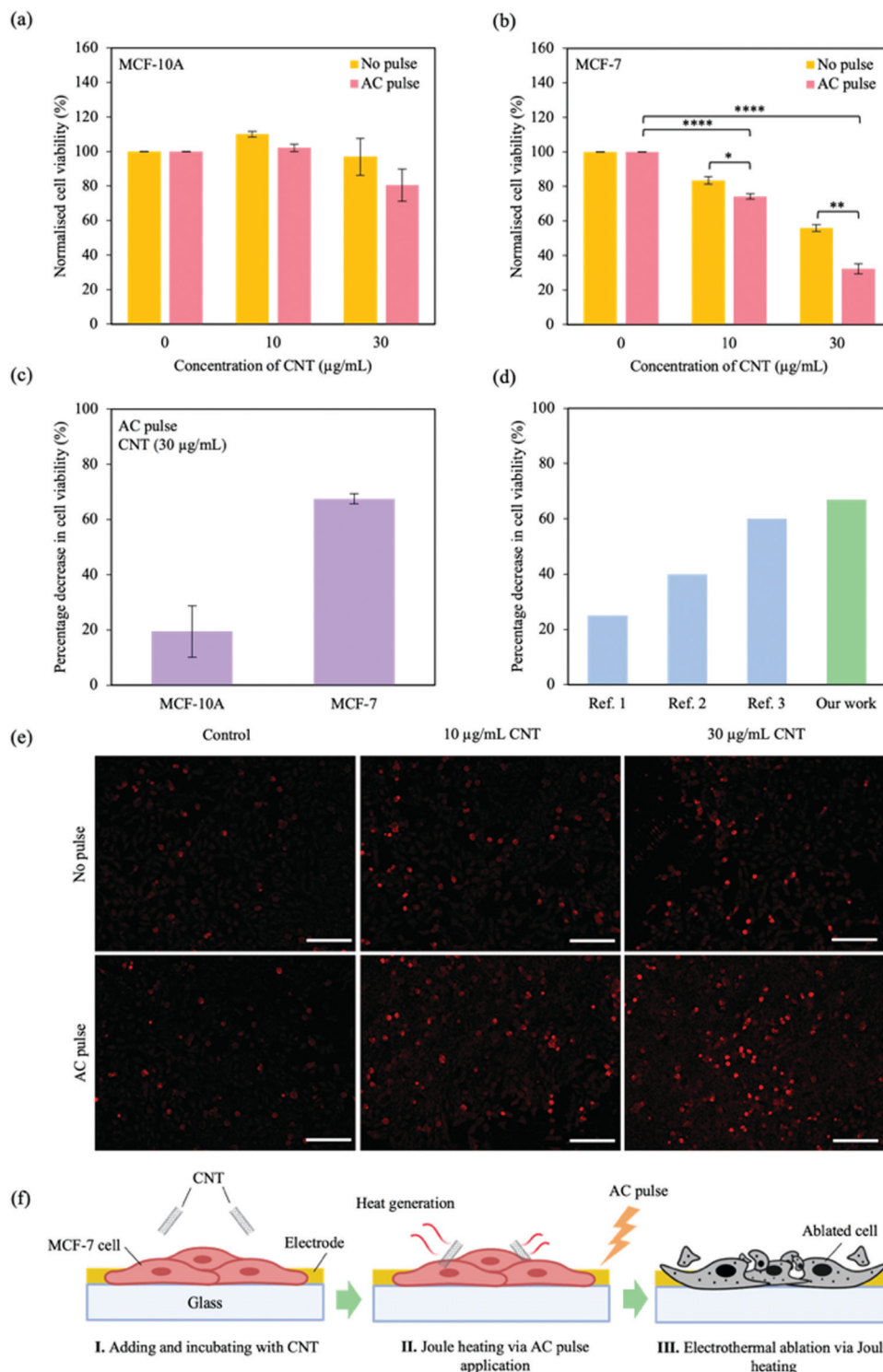
Fig. 3 Ablating cancer cells through combined AC pulse and CNT materials effects. Normalised cell viability after AC pulse for (a) MCF-10A cells and (b) MCF-7 cells at different CNT concentrations (0, 10 and 30 μg mL^{-1}). Cell viability was determined using WST-1 assay and were normalised to control (no CNT incubation) with no pulse and with AC pulse. (c) Percentage decrease in cell viability for MCF-10A/CNT and MCF-7/CNT (30 μg mL^{-1}) after applying AC pulses. Percentage decrease was calculated using Eqn 2. Data represent mean ± SEM, (n = 6 from 3 independent experiments). Significance was calculated using a Student's t-test and is presented as: $p < 0.05$ (*), $p < 0.01$ (**), $p < 0.001$ (***) and $p < 0.0001$ (****). Unmarked significance denotes non-significance. (d) Comparison of the percentage decrease in cell viability of the AC pulse CNT system with that of state-of-the-art, carbon-based photothermal nanoagents without additional chemotherapeutic drugs. The references are presented in Table S4 (ESI†). (e) Propidium iodide (PI) staining for MCF-7 cells ~24 h after AC pulse application. Cells were incubated with different CNT concentrations (0, 10 and 30 μg mL^{-1}). Scale bar, 200 μm. (f) Schematic illustration of the proposed electrothermal ablation process. I. CNT is introduced to the MCF-7 cells and incubated for ~24 h, II. AC pulses are applied to the set up, resulting in Joule heating of the CNT and a rise in temperature within the MCF-7 cells, and III. MCF-7 cells are ablated as a result of Joule heating.
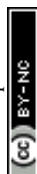
incubated with CNT with AC pulse for a specified concentration of CNT. We observed a percentage decrease in cell viability of ~68% for MCF-7 cells incubated with 30 μg mL^{-1} of CNT and exposed to AC pulse, higher than that for MCF-10A cells under the same conditions (~20%, Fig. 3c).

Additionally, fluorescent staining of dead cells was performed with propidium iodide (PI); PI chelates to nucleic acids and is not permeable to living cells. As cells undergo cell death, the cell membrane becomes permeable and PI can enter the cell and fluoresce red. As a result, PI is utilized to quantitatively discriminate dead cells from live cells.[47,48] For a high population of dead cells, the region of fluorescence is large, while a small fluorescence region is observed for a low dead-cell population. Cells were incubated with PI ~24 h after electrical application and fixed with paraformaldehyde (PFA). Fig. 3e shows MCF-7 cells after PI incubation and fixation for different CNT concentrations and applied AC pulse. We observed an increasing fluorescence region with increasing CNT concentration and the application of AC pulses, and is highest when cells were incubated with 30 μg mL^{-1} CNT and exposed to AC pulses. For normalised cell viability of MCF-7 cells at different CNT concentrations (Fig. 3b), experiments have demonstrated that increasing CNT concentrations result in a decreasing cell viability. When an AC pulse is injected, the cell viability of MCF-7 cells with high CNT concentrations further decreases. This trend is also observed for the PI staining of MCF-7 cells (Fig. 3e); when low CNT concentrations are utilised, a weak fluorescence signal is observed indicating high cell viability. As CNT concentration increases, MCF-7 cells showed a stronger fluorescence signal. The fluorescence signal intensity of MCF-7 cells with high CNT concentrations further increased when an AC pulse is administered. These findings agree well with the results in Fig. 3b. For MCF-10A cells (Fig. 3a), the normalised cell viability does not significantly change for different concentrations of CNT/pulsing conditions. After PI staining MCF-10A cells under different CNT concentrations/pulsing conditions (Fig. S5, ESI†), the fluorescence signal continues to be weak/negligible, in agreement with the findings in Fig. 3a.

Using the proposed system, we demonstrate a ~68% decrease in cell viability, above an average of ~40% decrease in cell viability for state-of-the-art, carbon-based photothermal (PT) nanoagents without additional chemotherapeutic drugs (Fig. 3d).[49–51] We propose a three-step electrothermal ablation process using the CNT AC pulse platform: I. CNT is introduced to the MCF-7 cells and incubated for ~24 h, allowing for CNT-cell interaction, II. AC pulses are applied to the set up, resulting in Joule heating of the CNT and a rise in temperature within the MCF-7 cells, and III. MCF-7 cells are ablated as a result of CNT Joule heating (Fig. 1a and 3f).

Joule heating describes the effect whereby an input of electrical energy is transformed into heat. This effect in CNTs occur when electrical energy from the charge carriers in the nanotube transfer to the vibrational modes (phonons) of the substrate, resulting in heat generation.[65,66] Thus, CNTs are promising materials for Joule heating applications such as thermal management[52–54] and additives in fabrics for sensors

and heating devices.[34,55] However, electrothermal ablation *via* Joule heating using CNT-based systems have yet to be investigated. CNTs have excellent electrical and thermal conductivity compared to other carbon-based nanomaterials.[27] Moreover, CNT can align themselves along the direction of an AC electric field.[56,57] While CNT alignment can improve the electrothermal conductivity,[58] the movement of CNT could also contribute to cell death *via* shear force to improve therapeutic efficiency substantially. We propose this system as a highly-efficient, high-specificity method of electrothermal ablation for clinically relevant applications.

MCF-7 cells were observed to be more sensitive to the as-prepared CNT compared to the MCF-10A cells; increased CNT cytotoxicity and electrothermal ablation. This could be due to the different cell membrane compositions between healthy and cancer cells that leads to differences in structural and mechanical properties. During cancer cell development, the cell division process is accelerated, resulting in shorter and less ordered actin fibres and a sparse cell membrane in cancer cells.[59–62] Actin fibres are an important component of the cell membrane, and accounts for cell membrane behaviour and mechanical integrity. Cancerous cells have been observed to be more easily deformed/less stiff than their healthy counter parts; measurements performed on MCF-10A cells demonstrate a significantly higher Young's modulus than MCF-7 cells.[59,60,63] This change in mechanical properties could result in the MCF-7 cell-specific CNT interaction. Because the MCF-7 cell membrane is softer and more fluid than the MCF-10A cell membrane, and hydrophobic CNTs can bury themselves within the hydrophobic tails of the cell membrane,[64–69] CNTs could be more easily embedded within the MCF-7 cell membrane compared to MCF-10A cell membranes. Since CNT is key to converting the applied AC pulse into heat, stronger CNT-cell interactions will enhance the heating effects in MCF-7 cells compared to that in MCF-10A cells, resulting in a larger MCF-7 cell ablation.

Discussion

The proposed system is advantageous over traditional thermal ablation methods as it requires a low nanomaterial concentration, less preparation time and a shorter ablation exposure time, reducing negative side effects and minimising therapy time. Cell-specific targeting is fundamental to increase efficiency and safety in cancer therapeutics; research in this field has been devoted to discovering facile methods for site-specific delivery. Traditional methods of cell-specific targeting include functionalising delivery agents with cell-specific antibodies such as mucin-1 (Muc-1) for breast cancer cells or epithelial adhesion molecule (EpCAM), which are overexpressed for most epithelial cancer cells.[17,70,71] However, these methods can be time consuming, requires multi-step preparations and a certain level of expertise. In this work, the system employs as-prepared, sonicated CNTs that demonstrates MCF-7 cancer cell-specific targeting. Moreover, traditional thermal ablation methods

requires high nanoagent concentrations (>50 μg mL^{-1}) and light exposure within minutes (<5 min) to achieve efficient thermal ablation.[72,73] On the other hand, this method requires exposing cells to low CNT concentrations within a second timescale. We demonstrate MCF-7 cell-specific electrothermal ablation, enhanced by a low concentration of CNT materials, while maintaining the cell viability for MCF-10A cells. Besides, a 68% decrease in cell viability was achieved upon the application of AC pulses, which is above the average of $\sim 40\%$ decrease in cell viability for current carbon-based photothermal nanoagents without additional chemotherapeutic drugs (Fig. 3d). This enables a larger population of cells to be ablated for substantially enhancing treatment efficacy. Thus, we propose the CNT AC pulse system as an alternative, highly-efficient, fast and simple-to-implement method that can specifically target and ablate MCF-7 cancer cells.

Due to the complexity of the CNT-cell interaction, the mechanisms by which CNT is internalised, distributed and cleared within various cell types are still not well understood. While some studies show that CNT spontaneously diffuses across the cell membrane,[74,75] other researchers demonstrate an energy-dependant mechanism for CNT internalisation (endocytosis).[42,76,77] Moreover, these mechanisms appear to be influenced by the structural properties of CNT (nanotube length and diameter, chirality), CNT functionalisation and cell type.[78–81] These factors can also affect CNT degradation, biodistribution and clearance;[80,82,83] the time it takes for CNT to clear the body can depend on the nanotube size, functionalisation group and degree of functionalisation.[84,85] Experimental *in vitro* and *in vivo* studies show that CNTs can be degraded by peroxidase enzymes, such as myeloperoxidase, eosinophil peroxidase and lactoperoxidase.[83,86,87] Further research in this area can provide a clearer picture of CNT internalisation and clearance mechanisms to ensure a balance between CNT retention in cancer cells and clearance in their healthy counterparts to reduce undesirable side effects.

Further studies could demonstrate the different CNT-cell interactions between CNT and cancerous and healthy cells. To determine the CNT internalisation pathway for MCF-7 cells and MCF-10A cells, cells could be incubated with CNT at different temperatures. This can be achieved by reducing incubating temperatures from 37 °C to 4 °C and determining the location of CNT; *e.g.*, CNTs found within the cells at low incubation temperatures suggest internalisation *via* energy-independent pathways.[74,76,77] Bioimaging could provide more information on how the combination of CNT and AC pulse affect the MCF-10A cells and MCF-7 cells. CNTs could be functionalised with fluorescent probes and imaged after incubation;[77,78] this could elucidate the location and distribution of CNTs within the different cell types. Alternative imaging methods, such as transmission electron microscopy (TEM), have also been used to determine CNT location *in vitro*.[68,88] Besides, further work could be performed on heterogenous 3D cell scaffolds to mimic tumors found within tissues. This could demonstrate the therapeutic efficiency of thermal ablation using the proposed AC pulse CNT platform *in vivo*.

Conclusion

Cancer cell-specific and effective electrothermal ablation was achieved with a combined AC pulse CNT platform through enhanced Joule heating effects that altered the thermal distribution of cell systems. We observed an MCF-7 cell-specific CNT cytotoxicity, which produced highly efficient electrothermal ablation, while maintaining the viability of MCF-10A cells. Furthermore, a $\sim 68\%$ decrease in cell viability was observed, above an average of $\sim 40\%$ decrease in cell viability for state-of-the-art photothermal nanoagents without additional chemotherapeutic drugs. The proposed system, which is highly-efficient, fast and simple to implement, presents the first application of CNT for clinically relevant electrothermal cancer cell ablation.

Data availability

The authors declare that data supporting the finding of this study are available within the article and the ESI.† Other data are available from the corresponding authors upon reasonable request.

Conflicts of interest

The authors declare no competing interests.

Acknowledgements

References

1 H. Sung, J. Ferlay, R. L. Siegel, M. Laversanne, I. Soerjomataram, A. Jemal and F. Bray, *CA. Cancer J. Clin.*, 2021, **71**, 209–249.

2 P. Jeyamohan, T. Hasumura, Y. Nagaoka, Y. Yoshida, T. Maekawa and D. S. Kumar, *Int. J. Nanomed.*, 2013, **8**, 2653.

3 P. Li, Y. Shi, B. Li, W. Xu, Z. Shi, C. Zhou and S. Fu, *J. Nanobiotechnology 2015 131*, 2015, **13**, 1–8.

4 E. A. Hussein, M. M. Zagho, G. K. Nasrallah and A. A. Elzatahry, *Int. J. Nanomed.*, 2018, **13**, 2897.

5 S. Cai, J. Yan, H. Xiong, Q. Wu, H. Xing, Y. Liu, S. Liu and Z. Liu, *Int. J. Pharm.*, 2020, **590**, 119948.

6 C. J. Diederich, *Int. J. Hyperth.*, 2005, **21**, 745–753.

7 J. R. Lepock, H. E. Frey and K. P. Ritchie, *J. Cell Biol.*, 1993, **122**, 1267.

8 Q. Li, H. Ruan and H. Li, *Pharm. Nanotechnol*, 2014, **2**, 58–64.

9 X. Xie, X. Shao, F. Gao, H. Jin, J. Zhou, L. Du, Y. Zhang, W. Ouyang, X. Wang, L. Zhao, X. Zhang and J. Tang, *Oncol. Rep.*, 2011, **25**, 1573–1579.

10 D. An, J. Fu, B. Zhang, N. Xie, G. Nie, H. Ågren, M. Qiu and H. Zhang, *Adv. Funct. Mater.*, 2021, **31**, 2101625.

11 F. Scopelliti, A. Pea, R. Conigliaro, G. Butturini, I. Frigerio, P. Regi, A. Giardino, H. Bertani, M. Paini, P. Pederzoli and R. Girelli, *Surg. Endosc. 2018 329*, 2018, **32**, 4022–4028.

12 D. E. Dupuy, W. W. Mayo-Smith, G. F. Abbott and T. DiPetrillo, *Radiographics*, 2002, **22**, S259–S269.

13 H. K. Lim, S. J. Cho, J. H. Baek, K. D. Lee, C. W. Son, J. M. Son and S. M. Baek, *Korean J. Radiol*, 2019, **20**, 1653–1661.

14 K. H. Son, J. H. Hong and J. W. Lee, *Int. J. Nanomed.*, 2016, **11**, 5163.

15 W. Yin, L. Yan, J. Yu, G. Tian, L. Zhou, X. Zheng, X. Zhang, Y. Yong, J. Li, Z. Gu and Y. Zhao, *ACS Nano*, 2014, **8**, 6922–6933.

16 B. Ortiz-Casas, A. Galdámez-Martínez, J. Gutiérrez-Flores, A. Baca Ibañez, P. Kumar Panda, G. Santana, H. A. de la Vega, M. Suar, C. Gutiérrez Rodelo, A. Kaushik, Y. Kumar Mishra and A. Dutt, *Mater. Today*, 2021, **50**, 533–569.

17 D. K. Loke, G. J. Clausen, J. F. Ohmura, T. C. Chong and A. M. Belcher, *ACS Appl. Nano Mater.*, 2018, **12**, 6556–6562.

18 L. Li, A. M. Belcher and D. K. Loke, *Nanoscale*, 2020, **12**, 24214–24227.

19 S. S. Chan, D. Lee, M. P. Meivita, L. Li, Y. S. Tan, N. Bajalovic and D. K. Loke, *Nanoscale Adv.*, 2021, **3**, 6974–6983.

20 J. R. Lee, S. Ryu, S. Kim and B. S. Kim, *Biomater. Res.*, 2015, **19**, 1–6.

21 P. Avouris, M. Freitag and V. Perebeinos, *Nat. Photonics*, 2008, **2**, 341–350.

22 X. He, F. Léonard and J. Kono, *Adv. Opt. Mater.*, 2015, **3**, 989–1011.

23 K. A. Shah, M. Shunaid Parvaiz and G. N. Dar, *Phys. Lett. Sect. A Gen. At. Solid State Phys*, 2019, **383**, 2207–2212.

24 L. V. Nair, Y. Nagaoka, T. Maekawa, D. Sakthikumar and R. S. Jayasree, *Small*, 2014, **10**, 2771–2775.

25 C.-L. Pai, Y.-C. Chen, C.-Y. Hsu, H.-L. Su and P.-S. Lai, *J. Biomed. Nanotechnol.*, 2016, **12**, 619–629.

26 A. R. Burke, R. N. Singh, D. L. Carroll, J. C. S. Wood, R. B. D'Agostino, P. M. Ajayan, F. M. Torti and S. V. Torti, *Biomaterials*, 2012, **33**, 2961–2970.

27 Z. Han and A. Fina, *Prog. Polym. Sci.*, 2011, **36**, 914–944.

28 A. H. Ghobadi, M. Armin, S. G. Hassankolaei and M. Gholinia Hassankolaei, *Int. J. Ambient Energy*, 2020, 1–12.

29 F. Deng, Q. S. Zheng, L. F. Wang and C. W. Nan, *Appl. Phys. Lett.*, 2007, **90**, 021914.

30 A. T. Chien, S. Cho, Y. Joshi and S. Kumar, *Polymer*, 2014, **55**, 6896–6905.

31 M. K. Smith, V. Singh, K. Kalaitzidou and B. A. Cola, *ACS Appl. Mater. Interfaces*, 2016, **8**, 14788–14794.

32 F. Schütt, S. Signetti, H. Krüger, S. Röder, D. Smazna, S. Kaps, S. N. Gorb, Y. K. Mishra, N. M. Pugno and R. Adelung, *Nat. Commun. 2017 81*, 2017, **8**, 1–10.

33 F. Schütt, F. Rasch, N. Deka, A. Reimers, L. M. Saure, S. Kaps, J. Rank, J. Carstensen, Y. Kumar Mishra, D. Misseroni, A. Romani Vázquez, M. R. Lohe, A. Shaygan Nia, N. M. Pugno, X. Feng and R. Adelung, *Mater. Today*, 2021, **48**, 7–17.

34 S. Noh and Y. Song, *Mech. Adv. Mater. Struct.*, 2020, 1–9.

35 J. Schindelin, I. Arganda-Carreras, E. Frise, V. Kaynig, M. Longair, T. Pietzsch, S. Preibisch, C. Rueden, S. Saalfeld, B. Schmid, J.-Y. Tinevez, D. J. White, V. Hartenstein, K. Eliceiri, P. Tomancak and A. Cardona, *Nat. Methods*, 2012, **9**, 676–682.

36 J. Yang, in *Thermal Conductivity: Theory, Properties and Applications*, ed. T. M. Tritt, 2005, p. 290.

37 M. Grujicic, G. Cao and B. Gersten, *Mater. Sci. Eng. B*, 2004, **107**, 204–216.

38 N. Shao, S. Lu, E. Wickstrom and B. Panchapakesan, *Nanotechnology*, 2007, **18**, 315101.

39 K. Shirasu, G. Yamamoto and T. Hashida, *Mater. Res. Express*, 2019, **6**, 055047.

40 R. K. Sahoo and C. Jacob, *Mater. Sci. Eng. B*, 2014, **185**, 99–104.

41 Y. Zhang, H. Gu, K. Suenaga and S. Iijima, *Chem. Phys. Lett.*, 1997, **279**, 264–269.

42 H. F. Cui, S. K. Vashist, K. Al-Rubeaan, J. H. T. Luong and F. S. Sheu, *Chem. Res. Toxicol.*, 2010, **23**, 1131–1147.

43 J. Kayat, V. Gajbhiye, R. Kumar Tekade and N. Kumar Jain, *Nanomedicine*, 2011, **7**, 40–49.

44 O. Vittorio, V. Raffa and A. Cuschieri, *Nanomedicine*, 2009, **5**, 424–431.

45 A. Shvedova, V. Castranova, E. Kisin, D. Schwegler-Berry, A. Murray, V. Gandelsman, A. Maynard and P. Baron, *J. Toxicol. Environ. Heal. Part A*, 2003, **66**, 1909–1929.

46 E. Esfandiary, A. Valiani, B. Hashemibeni, I. Moradi and M. Narimani, *Adv. Biomed. Res.*, 2014, **3**, 40.

47 L. C. Crowley, A. P. Scott, B. J. Marfell, J. A. Boughaba, G. Chojnowski and N. J. Waterhouse, *Cold Spring Harb. Protoc.*, 2016, **2016**, 647–651.

48 Y. Zou, M. Li, T. Xiong, X. Zhao, J. Du, J. Fan, X. Y. Peng Zou, M. Li, T. Xiong, X. Zhao, J. Du, J. Fan and X. Peng, *Small*, 2020, **16**, 1907677.

49 Y. Wang, H. Wang, D. Liu, S. Song, X. Wang and H. Zhang, *Biomaterials*, 2013, **34**, 7715–7724.

50 J. Liu, C. Wang, X. X. Wang, X. X. Wang, L. Cheng, Y. Li and Z. Liu, *Adv. Funct. Mater.*, 2015, **25**, 384–392.

51 A. Sahu, W. Il Choi, J. H. Lee and G. Tae, *Biomaterials*, 2013, **34**, 6239–6248.

52 K. H. Baloch, N. Voskanian, M. Bronsgeest and J. Cumings, *Nat. Nanotechnol. 2012 75*, 2012, **7**, 316–319.

53 H. Huang, C. H. Liu, Y. Wu and S. Fan, *Adv. Mater.*, 2005, **17**, 1652–1656.

54 T. Ragab and C. Basaran, *J. Appl. Phys.*, 2009, **106**, 063705.

55 M. O. Faruk, A. Ahmed, M. A. Jalil, M. T. Islam, A. M. Shamim, B. Adak, M. M. Hossain and S. Mukhopadhyay, *Appl. Mater. Today*, 2021, **23**, 101025.

56 K. Bubke, H. Gnewuch, M. Hempstead, J. Hammer and M. L. H. Green, *Appl. Phys. Lett.*, 1998, **71**, 1906.

57 X. Q. Chen, T. Saito, H. Yamada and K. Matsushige, *Appl. Phys. Lett.*, 2001, **78**, 3714.

58 Q. Wang, J. Dai, W. Li, Z. Wei and J. Jiang, *Compos. Sci. Technol.*, 2008, **68**, 1644–1648.

59 Y. Wang, C. Xu, N. Jiang, L. Zheng, J. Zeng, C. Qiu, H. Yang and S. Xie, *Scanning*, 2016, **38**, 558–563.

60 Y. Nematbakhsh, K. T. Pang and C. T. Lim, *Converg. Sci. Phys. Oncol.*, 2017, **3**, 034003.

61 A. Heydarian, D. Milani and S. M. Moein Fatemi, *Biochem. Biophys. Res. Commun.*, 2020, **529**, 432–436.

62 N. Schierbaum, J. Rheinlaender and T. E. Schäffer, *Acta Biomater.*, 2017, **55**, 239–248.

63 Q. S. Li, G. Y. H. Lee, C. N. Ong and C. T. Lim, *Biochem. Biophys. Res. Commun.*, 2008, **374**, 609–613.

64 R. Parthasarathi, N. R. Tummala and A. Striolo, *J. Phys. Chem. B*, 2012, **116**, 12769–12782.

65 M. N. Al-Qattan, P. K. Deb and R. K. Tekade, *Drug Discovery Today*, 2018, **23**, 235–250.

66 M. Lelimousin and M. S. P. Sansom, *Small*, 2013, **9**, 3639–3646.

67 B. J. Panessa-Warren, J. B. Warren, S. S. Wong and J. A. Misewich, *J. Phys. Condens. Matter*, 2006, **18**, S2185–S2201.

68 C. Cheng, A. E. Porter, K. Muller, K. Koziol, J. N. Skepper, P. Midgley and M. Welland, *J. Phys.: Conf. Series*, 2009, **151**, 012030.

69 A. E. Porter, M. Gass, K. Muller, J. N. Skepper, P. A. Midgley and M. Welland, *Nat. Nanotechnol.*, 2007, **2**, 713–717.

70 N. Berois, M. Varangot, B. Aizen, R. Estrugo, L. Zarantonelli, P. Fernández, G. Krygier, F. Simonet, E. Barrios, I. Musé and E. Osinaga, *Eur. J. Cancer*, 2000, **36**, 717–723.

71 S.-G. Shiah, K.-Y. Tai and C.-W. Wu, *J. Cancer Mol*, 2008, **3**, 165–168.

72 L. M. Tu Phan, A. Rana Gul, T. Ngoc Le, M. Woo Kim, S. Kumar Kailasa, K. Taek Oh and T. Jung Park, *Biomater. Sci.*, 2019, **7**, 5187–5196.

73 X. Liang, W. Shang, C. Chi, C. Zeng, K. Wang, C. Fang, Q. Chen, H. Liu, Y. Fan and J. Tian, *Cancer Lett.*, 2016, **383**, 243–249.

74 A. Bianco, K. Kostarelos and M. Prato, *Curr. Opin. Chem. Biol.*, 2005, **9**, 674–679.

75 W. Yang, P. Thordarson, J. J. Gooding, S. P. Ringer and F. Braet, *Nanotechnology*, 2007, **18**, 12.

76 H. Xiao, L. Yang, H. Zou, L. Yang and X. C. Le, *Anal. Bioanal. Chem.*, 2007, **387**, 119–126.

77 N. W. S. Kam, M. O'Connell, J. A. Wisdom and H. Dai, *Proc. Natl. Acad. Sci. U. S. A.*, 2005, **102**, 11600–11605.

78 K. Kostarelos, L. Lacerda, G. Pastorin, W. Wu, S. Wieckowski, J. Luangsivilay, S. Godefroy, D. Pantarotto, J.-P. Briand, S. Muller, M. Prato and A. Bianco, *Nat. Nanotechnol. 2007 22*, 2007, **2**, 108–113.

79 L. Lacerda, S. Raffa, M. Prato, A. Bianco and K. Kostarelos, *Nano Today*, 2007, **2**, 38–43.

80 Z. Liu, J. T. Robinson, S. M. Tabakman, K. Yang and H. Dai, *Mater. Today*, 2011, **14**, 316–323.

81 A. Facciolà, G. Visalli, S. La Maestra, M. Ceccarelli, F. D'Aleo, G. Nunnari, G. F. Pellicanò and A. Di Pietro, *Environ. Toxicol. Pharmacol.*, 2019, **65**, 23–30.

82 K. D. Patel, R. K. Singh and H.-W. Kim, *Mater. Horiz.*, 2019, **6**, 434–469.

83 P. M. Costa, M. Bourgognon, J. T. W. Wang and K. T. Al-Jamal, *J. Control. Release*, 2016, **241**, 200–219.

84 Z. Liu, C. Davis, W. Cai, L. He, X. Chen and H. Dai, *Proc. Natl. Acad. Sci. U. S. A.*, 2008, **105**, 1410–1415.

85 R. Singh, D. Pantarotto, L. Lacerda, G. Pastorin, C. Dric Klumpp, M. Prato, A. Bianco and K. Kostarelos, *Proc. Natl. Acad. Sci. U. S. A.*, 2006, **103**, 3357–3362.

86 M. Chen, X. Qin and G. Zeng, *Trends Biotechnol.*, 2017, **35**, 836–846.

87 G. P. Kotchey, Y. Zhao, V. E. Kagan and A. Star, *Adv. Drug Delivery Rev.*, 2013, **65**, 1921–1932.

88 D. Pantarotto, R. Singh, D. McCarthy, M. Erhardt, J. P. Briand, M. Prato, K. Kostarelos and A. Bianco, *Angew. Chem., Int. Ed.*, 2004, **43**, 5242–5246.